

Thermal Aging Based Degradation Parameters Determination for Grid-Aged Oil Paper Insulation

Basu, Devayan; Gholizad, Babak; Ross, Rob; Gargari, Shima Mousavi

DOI

[10.1109/TDEI.2022.3217434](https://doi.org/10.1109/TDEI.2022.3217434)

Publication date

2022

Document Version

Accepted author manuscript

Published in

IEEE Transactions on Dielectrics and Electrical Insulation

Citation (APA)

Basu, D., Gholizad, B., Ross, R., & Gargari, S. M. (2022). Thermal Aging Based Degradation Parameters Determination for Grid-Aged Oil Paper Insulation. *IEEE Transactions on Dielectrics and Electrical Insulation*, 30(2), 734-743. <https://doi.org/10.1109/TDEI.2022.3217434>

Important note

To cite this publication, please use the final published version (if applicable).
Please check the document version above.

Copyright

Other than for strictly personal use, it is not permitted to download, forward or distribute the text or part of it, without the consent of the author(s) and/or copyright holder(s), unless the work is under an open content license such as Creative Commons.

Takedown policy

Please contact us and provide details if you believe this document breaches copyrights.
We will remove access to the work immediately and investigate your claim.

Thermal Aging Based Degradation Parameters Determination for Grid-Aged Oil Paper Insulation

Devayan Basu, Babak Gholizad, Rob Ross, IEEE Member, Shima Mousavi Gargari

Abstract— Elevated thermal stress related aging is significant on the oil impregnated paper(OIP) used as insulation in high-pressure gas cables (HPGC). The aim of this paper is to develop a cheap alternative for lab dielectric measuring and characterizing temperature dependent parameters for OIP. Firstly, this paper derives the operating thermal conditions of the grid-aged cable based on IEC Standards after analyzing the loading data using machine learning techniques to determine the elevated temperature levels for the experiments. Secondly, a novel lab fabricated inexpensive electronics circuit is developed for polarization and depolarization current measurements which can be adapted for such measurements over expensive commercial devices. From the measured parameters, an extended 3 branch Debye model is optimized using a developed Error Function approach based on Akaike Information Criterion and goodness of fit. The model indicated a reduction in the branch resistance with temperature elevation and aging, whereas the branch capacitance revealed an increasing trend. The resultant relaxation time(RC) showed a decrease overall. Lastly, a short-duration frequency domain spectrum was analyzed and extrapolated to obtain parameters for a wide range of frequencies and fitted in a Cole-Cole model, derived for oil-paper insulation. The time constants obtained from this model also confirmed a reducing trend across the temperature and aging variations and the model parameter, the alpha coefficient showed a decreasing trend. Lastly, the effect of the measured dielectric parameters is reflected with breakdown values to investigate the effect of temperature on electrical life of insulation.

Index Terms— Aging, Cole-Cole Model, Extended Debye Model, Frequency Dielectric Spectroscopy, Oil Impregnated Paper (OIP), Polarization/ Depolarization, Thermal Stress

1. INTRODUCTION

MONITORING and assessing the condition of cable insulation has become a growing area of research. Due to the nature of the non-destructive tests that are needed to be performed, one is often limited to assess degradation in field conditions. High Pressure Gas Cables (HPGC) have been installed about 40 years ago by TenneT, the transmission system operator (TSO) of the Netherlands and parts of Germany. Due to thermal and electrical aging over 40 years, these HPGCs are at the end of life and must be replaced,

but on a priority basis. To investigate the cable insulation condition, indications for relative degradation rate need to be investigated. Therefore, a robust model should be developed using the measurements with the least cable outage time and without aging the insulation further. For diagnostics, the experiments are preferred to be with or below operation conditions. This is because, during offline partial discharge measurement, the cable is exposed to voltages higher than the nominal voltage ($1.7U_0$), which may expose the already aged cables to faster aging. For FDS measurements, a long range of frequencies is normally used, but high-frequency measurement has a high current requirement, increasing the measuring equipment size as well as the issue of taking the cable out of operation which interrupts service for a considerable time.

There has been significant research on polarization and depolarization current (PDC) measurement [1-13] and frequency dielectric spectroscopy (FDS), including the influence of aging and moisture on oil-impregnated paper [14-19]. But a majority of research has been based on oil-paper pressboards used in transformers or artificial oil impregnation of kraft paper. Also, from the material perspective, multiple polarization events occur during DC voltage application, but the tradeoff between the goodness of fit, the number of model variables, and complexity often become difficult to quantify. Therefore, there is a need for mathematical criteria to model the optimal number of polarization branches, which will help to determine intrinsic insulation properties.

This paper aims to extract model parameters for quantifying the effect of elevated thermal stress on grid-aged HPGC samples. The paper is divided into 6 sections and in Section 2, the operating temperature of the grid-aged HPGC insulation is derived from the loading data supplied by TenneT TSO after treating the data for anomalies using machine learning. Section 3 discusses the preparation of the electrodes and samples depending on the applied thermal stresses. Section 4 reports the PDC measurement system developed in the lab to have reliable switching between the two events leading to the development of the Debye model based on the Akaike Information Criteria and goodness of fit. The section also discusses the trends in the measured parameters with thermal stress and aging. Section 5 describes the FDS measurement and trends in the measured parameters observed for the prepared

This work was supported financially by TenneT TSO, Netherlands. The authors would like to acknowledge Dr. Luis Heredia, Geert Jan Kamphuis and Wim Termorshuizen for their help in building the experimental setups and in manufacturing parts in the workshop.

D.Basu was with Technical University of Delft, Netherlands, Mekelweg 4, 2628CD Delft in the Department of Electrical Engineering under High Voltage Specialization. Now he is affiliated to ETH Zurich, Switzerland, Physikstrasse 3, 8092 in the High Voltage Laboratory Group focusing on gaseous insulation. (e-mail: basu@eeh.ee.ethz.ch)

B.Gholizad was with Technical University of Delft, Netherlands, Mekelweg 4, 2628CD Delft and now working with TenneT TSO, 428 6800 AK Arnhem, Netherlands. (e-mail: B.Gholizad@tudelft.nl)

R.Ross is Full Professor in the Department of Electrical Engineering in Technical University of Delft, Netherlands, Mekelweg 4, 2628CD Delft. He is also working in Asset Management Team in TenneT TSO, 428 6800 AK Arnhem, Netherlands. (e-mail: Rob.Ross@tudelft.nl)

S.M.Gargari is currently working as an Asset Technologist Responsible for cables system for AC and DC in TenneT TSO, 428 6800 AK Arnhem, Netherlands. (e-mail: Shima.MousaviGargari@tennet.eu)

samples which form the basis of input parameters to the modified Cole-Cole model. Finally, conclusions are made in Section 6 based on the parameters obtained from Sections 4 and 5 to assess the possibility of comparing insulation conditions in thermally aged HPGC samples.

2. OPERATING TEMPERATURE OF HPGC

The loading profile of the HPGC was collected from TenneT for 6 years at an interval of 5 minutes, which contained some erroneous data, that may be arising from the sensor. This loading data was first cleaned, anomalies were detected and treated by the Isolation Forest Algorithm [20] as shown in Figure 1(top). On this loading dataset, IEC-60287-1/2-1[21-22] was implemented to establish the relationship between the conductor temperature and loading which was smoothed by moving average to obtain the dynamic temperature plot seen in Figure 1(bottom).

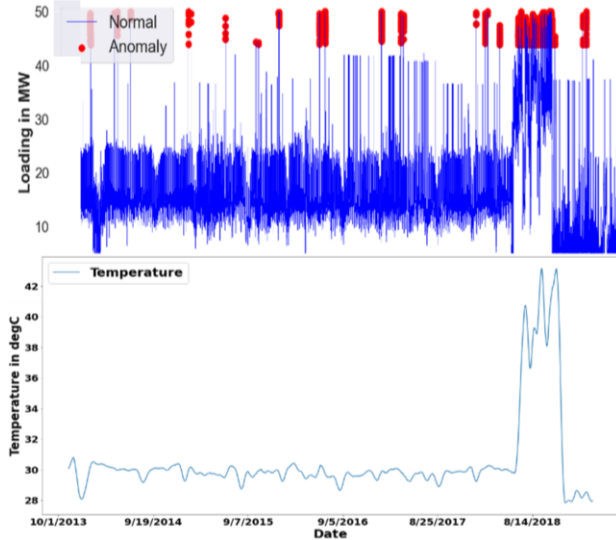


Fig. 1. Data processing to determine operational temperature. It can be observed that the temperature remains almost constant at 30°C, but due to an event in one of the parallel lines, the cable was overloaded during 08/2018, rising conductor temperature higher than 42°C, which was also confirmed by TenneT.

3. ELECTRODES AND SAMPLE PREPARATION

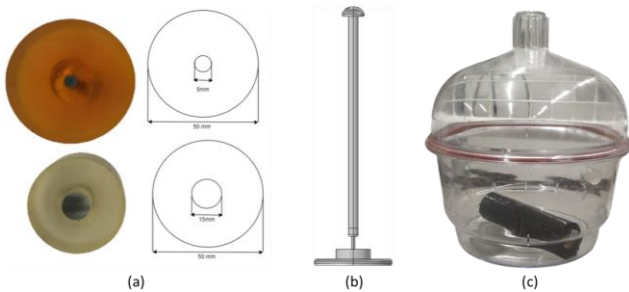


Fig. 2. (a) Epoxy casted electrodes, (b) Model of the experimental setup, (c) Excess insulation storage

The electrodes used for PDC were made of stainless steel with a diameter of 15 mm and 5 mm for breakdown measurements. All the electrodes were cast in epoxy with an overall diameter 50 mm seen in Figure 2. No external oil was used, to not alter

the chemical properties of the oil used in the HPGC. The epoxy casting ensures that no partial discharge takes place during the application of the high voltage. Three different thicknesses of paper insulation as seen in Figure 3 were observed inside the cables. But the experiments were conducted with the inner layers of the least thickness since they are closest to the conductor which experiences maximum thermal and electrical stress.

The samples used for the experiment are single-layered OIP from a service-aged HPGC installed by TenneT TSO in the Netherlands with the following specifications in Table I:

TABLE I

TENNET SUPPLIED CABLE SPECIFICATIONS

Insulation Type	Nominal Line Voltage	Nominal Line Current	Nominal Power Rating	Maximum Designed Temperature
OIP	110 kV	570 A	108 MW	75°C

The samples are cut equally into 7cm×3cm rectangular pieces and the excess insulation to be used later is stored in a vacuum jar to prevent moisture ingress for a maximum period of 14 days. For the experiments, two types of samples are prepared: *Type 1- Aged Samples:* The samples are first kept at 75°C for 1 week to remove the moisture and then they are kept for 14 days at the specific temperatures of 45°C, 60°C, and 75°C. Thus, they undergo a total of around 500 hours of aging.

Type 2- Conditioned Samples: These samples are kept at 75°C for 1 week to remove any moisture and maintain equal levels for each one. Then they are kept at 45, 50, 60, and 75°C for 4 more days to condition them, with a total of 250 hours of aging. Let us define the term, “aging degree” as the duration of aging of the samples, and this term will be higher for aged samples compared to conditioned samples.

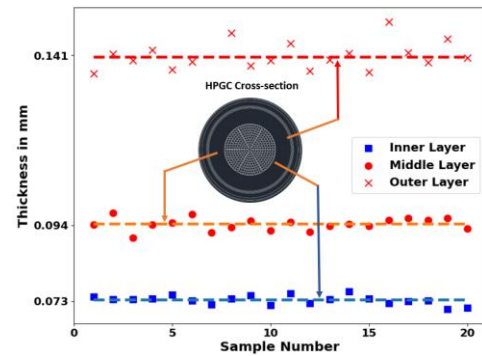


Fig. 3. Different layer thickness of insulation in cable

4. PRINCIPLE OF PDC MEASUREMENT AND RESULTS

Polarization, depolarization currents and the parameters derived from them using models is very vital in diagnosing the aging of polymer or oil-paper insulation in time domain [1-3]. Every insulation can be modeled as a capacitor and parallel resistance, C_0 and R_0 respectively. Firstly, a DC voltage of 1 kV (U_0) is applied to initiate the polarization process. This value is chosen such that the field is not sufficiently high to initiate electrical aging during the time of the experiment. The polarization process is carried out for 5000s after which the DC source is short-circuited initiating the depolarization process for the next 5000s [5,10]. During these two processes, polarization

and depolarization currents flow respectively in the order of magnitude of picoamperes, which are measured using Keithley 617 Programmable Electrometer. The measured data is logged using a MATLAB script via National Instrument GPIB bus. Figure 4 below depicts the connection diagram.

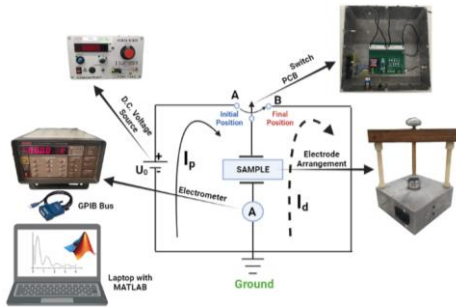


Fig. 4. Connection diagram for PDC measurement

An electronic circuit using Arduino Micro controlled 2 parallel NPN transistors is designed. This reduces the switching time to 3ms and eliminates the possibility of bouncing debouncing as in case of electromechanical relays which may cause unwanted transients. The lab implementation of the setup from development to testing along with the device control has been explained in [8] as can also be seen in Figure 5 showing the different electronic components. This inexpensive alternative has been benchmarked with XLPE samples which were measured by commercial DIRANA. The preliminary benchmark results revealed <5% difference between the 2 measurements validating the accuracy of the setup. The validation has been done for XLPE and OIP samples.

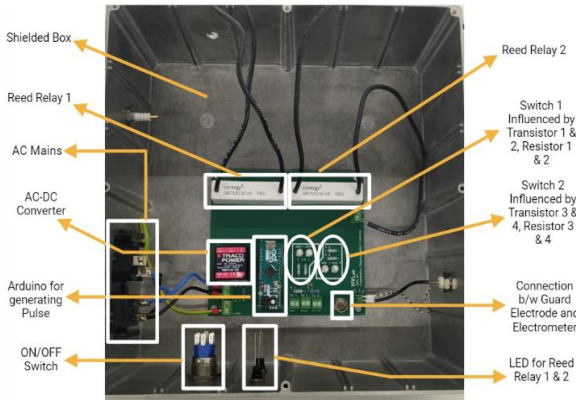


Fig. 5. Switching circuit for PDC measurement

A guarded electrode is used so that the surface leakage current is collected and shunted around the measuring instrument for accurate dielectric measurements. In the presence of the electric field, the current for the first 5000s (T_p) from time t_0 till t_1 can be seen in Figure 6(a), called the polarization current ($i_p(t)$) developed due to the tendency of dipoles to align in the direction of the field. When the field is removed, the dipoles de-align themselves causing the depolarization current ($i_d(t)$) to flow in the opposite direction [9] for next 5000s (T_d) as seen in Figure 6a. The response time of the cellulose groups after the application of an electric field may differ from one another. Thus, each polarization process can be modeled as a parallel circuit consisting of a series of R-C[2,7,9] shown in Figure 6(b) with corresponding branch names.

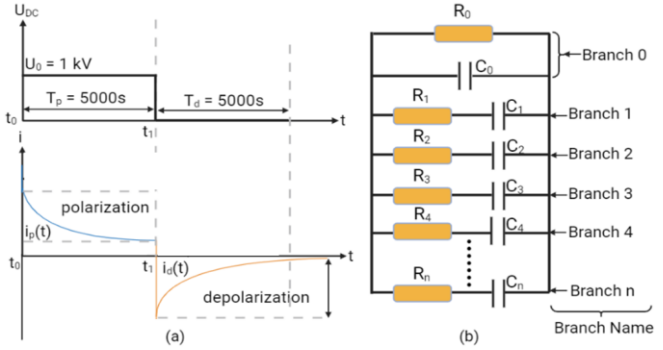


Fig. 6. (a) $i_p(t)$ and $i_d(t)$ variation with applied DC voltage, (b) R-C series branch representation of polarization processes

4.1. MATHEMATICAL FORMULATION OF THE MODEL

For a geometrical capacitance C_0 of the OIP sample and field strength $E(t)$ due to an external voltage $U(t)$, the current through a homogenous dielectric [3,6] can be expressed as Equation (1):

$$i(t) = C_0 \left[\frac{\sigma_0}{\epsilon_0} U(t) + \epsilon_\infty \frac{dU(t)}{dt} + \frac{d}{dt} \int_0^t \varphi(t-\tau) U(\tau) d\tau \right] \quad (1)$$

Where, ϵ_∞ denotes relative permittivity at a power frequency of 50Hz, $\varphi(t)$ represents the dielectric response function at time t . The measured polarization current (i_p) in this period contains both absorption and conduction currents [3], expressed as:

$$i_p(t) = C_0 U_0 \left[\frac{\sigma_0}{\epsilon_0} + \epsilon_\infty \delta(t) + \varphi(t) \right] \quad (2)$$

Where, $\delta(t)$ is the impulse voltage and U_0 is the applied DC voltage. Now, with the removal of the DC source, the sample is short-circuited allowing the flow of depolarization current (i_d), composed of only absorption current [3] and given by:

$$i_d(t) = -C_0 U_0 [\varphi(t) - \varphi(t + T_p)] \quad (3)$$

From the Extended Debye Model for modeling polarization processes inside the OIP Insulation, the depolarization current can be fitted by a series of exponentially decaying functions [7] given by:

$$I_d = \sum_{i=1}^n \alpha_i e^{-\frac{t}{\tau_i}} \quad (4)$$

Where, i stands for the polarization process, α_i is the constant coefficient and τ_i are the relaxation time constants. From these relaxation time constants, it is possible to extract the series resistance (R_i) and capacitance (C_i) branch values [9] in the model given by the following equations:

$$R_i = U_0 \left(1 - e^{-\frac{t}{\tau_i}} \right) / \alpha_i \quad (5)$$

$$C_i = \tau_i / R_i \quad (6)$$

The geometric branch resistance [9] can be approximated as:

$$R_0 \approx \frac{U_0}{i_p(t_m) - i_d(t_m)} \quad (7)$$

Where, $i_p(t_m)$ and $i_d(t_m)$ are the polarization and depolarization current values after 5000s respectively. C_0 is the geometric branch capacitance that has been calculated by measuring the capacitance at 50 Hz using IDAX 300 and dividing it by the real part of permittivity (ϵ') [2].

4.2. PROCESSING OF THE PDC EXPERIMENTAL DATA

For each setpoint, 3 sets of measurements are recorded from the MATLAB GUI and the following method was used for analyzing the PDC data:

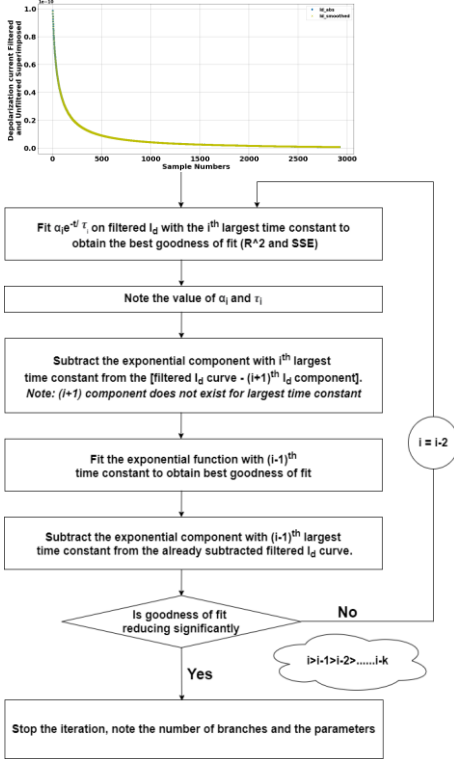
Step 1: Acquiring Unfiltered I_p and I_d in MATLAB:

The first 10 data points for both the processes are eliminated owing to the transients due to switching of the circuit [1]. I_p contains more noise compared to I_d due to induced noises from the DC source.

Step 2: Filtering the Signals:

The signals are passed through a Butterworth Filter coded in Python, to eliminate the high-frequency components. For selecting the filter order and critical frequency, a double loop was run such that the error between the filtered & unfiltered data was <1%. No physical filter was used since the difference between the two was small.

Step 3: Fitting the Extended Debye Model on Filtered I_d :



4.3. CHOOSING THE OPTIMAL NUMBER OF BRANCHES

It often becomes difficult to choose a model based on only the Sum of Squares of Errors and the R^2 Scores. Several instances arise when the R^2 score improvement is very insignificant at the expense of additional parameters. Also, a model with a smaller number of branches may not accurately model all the polarization processes. From the literature, it is observed that, for OIP insulation, 2-6 branches are the optimal fits [2,7,9]. To compensate for the increased complexity in the model leading to insignificant R^2 increment, the Akaike Information Criterion (AIC) [23] has been adjusted for the regression model. The log-likelihood maximization can be equated proportional to the minimization of the Sum of Squares of Errors (SSE). So, for regression-based applications, it is rewritten as:

$$\text{Adjusted AIC} = 2K - 2\ln(1/\text{SSE}) \quad (8)$$

Now, each Adjusted AIC value is divided by the Minimum AIC to obtain Normalized AIC. Now, let us define an Error Function, and the lower its value, the better is the model:

$$\text{Error Function} = [(1 - \text{Normalized AIC}) + (1 - \text{Adjusted } R^2)] * 100\% \quad (9)$$

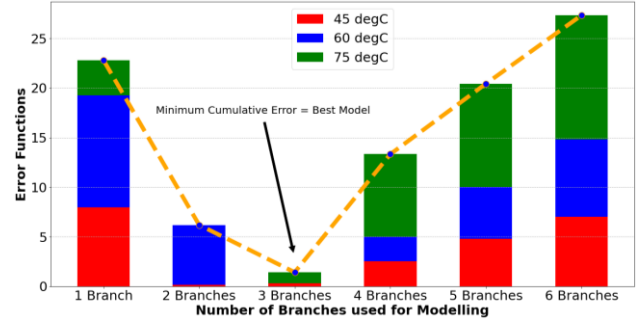


Fig 7. Error function for aged samples

For Aged (Figure 7) and Conditioned Samples represented in stacked bar graphs for different temperatures, it was observed that the error function reduces and reaches minimum for 3 branches and then starts to increase monotonically. Therefore, 3 branches have been used for modelling the polarization processes in the OIP samples.

4.4. TREND IN THE OIP INSULATION PARAMETER

4.4.1 TRENDS IN DC CONDUCTIVITY (κ)

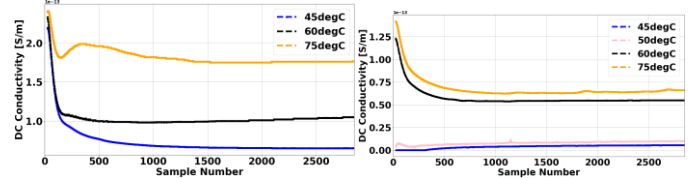
DC Conductivity (κ) of the dielectric can be formulated from Equations (2) and (3) as:

$$\sigma_0 \approx \frac{\epsilon_0}{C_0 U_0} [i_p(t) - i_d(t)] \quad (10)$$

With an increase in temperature for different degrees of aging, it is observed that κ increases as seen in Figure 8. Figures 8, 9 and 10 are plotted with 1 sample every 2 seconds. In OIP samples, the conductivity of insulating oil is exponentially proportional to temperature [11]:

$$\kappa = \kappa_0 \exp(-F/k_B T) \quad (11)$$

As insulation is aged, it is observed that κ increases. When the insulation is aged, the internal structure of the paper is altered e.g., thermal-oxidative aging [12], enhancing κ .

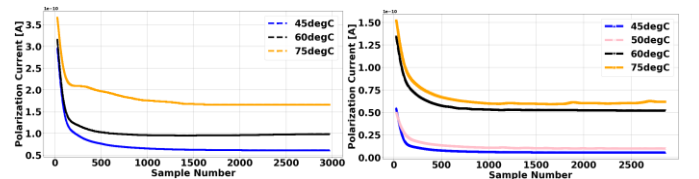


(a) Aged Samples (b) Conditioned Samples

Fig 8. Variation in κ with temperature and aging degree

4.4.2 TRENDS IN POLARIZATION CURRENT (I_p)

From Equation (2), it is evident that I_p is proportional to conductivity and real permittivity at very high frequencies. Now, with increase in temperature, κ increases (Section 4.4.1) and ϵ'_∞ also rises (Section 5.1.1), resulting in increase of I_p as shown in Figure 9. With increase in aging, κ increases and ϵ'_∞ increases, resulting in upward shift of I_p [7,9].



(a) Aged Samples (b) Conditioned Samples

Fig 9. Variation in I_p with temperature and aging degree

TABLE II
MODEL PARAMETERS FOR EACH BRANCH AT DIFFERENT TEMPERATURES

Temperature (°C)	Branch Number	$\tau_{\text{conditioned}}$ (sec)	τ_{aged} (sec)	$R_{\text{conditioned}}$ (TΩ)	R_{aged} (TΩ)	$C_{\text{conditioned}}$ (pF)	C_{aged} (pF)
45	Branch 0	1575	135	191.2	16.5	8.24	8.22
	Branch 1	2114	1450	385.0	293	5.49	4.94
	Branch 2	258	180	39.3	31.3	6.56	5.74
	Branch 3	53	45	18.3	12.7	2.89	3.56
60	Branch 0	161	85	19.5	10.3	8.24	8.23
	Branch 1	1350	1100	153.0	102	8.8	10.8
	Branch 2	180	170	23.9	20.4	7.52	8.33
	Branch 3	45	40	57.1	10.6	0.788	3.78
75	Branch 0	134	50	16.2	6.1	8.24	8.22
	Branch 1	900	850	112.0	47.2	8.05	18.0
	Branch 2	160	150	16.4	13.9	9.76	10.8
	Branch 3	40	35	67.0	8.32	5.97	4.24

4.4.3 TRENDS IN DEPOLARIZATION CURRENT (I_d)

In Equation 3, $\varphi(t + T_p) \approx 0$, it is short-circuited for a long duration of 1.5 hrs. The dielectric response time, $\varphi(t)$ varies continuously however after sufficient time when the discharging occurs, they settle at similar values, irrespective of temperature. The noticeable change is the rate of decay which varies depending on the amount of charge stored during polarization, for the aged sample is higher compared to conditioned samples. As temperature increases, slope reduces, which is very evident in the aged samples as seen in Figure 10.

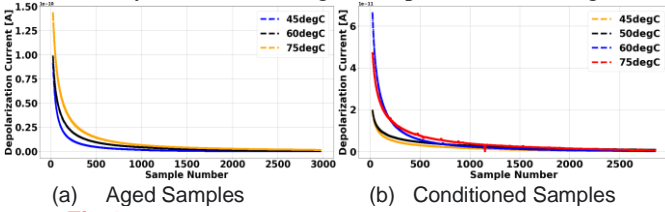


Fig 10. Variation in I_d with temperature and aging degree

4.5. TRENDS IN EXTENDED DEBYE MODEL DERIVED OIP INSULATION PARAMETERS

4.5.1 TRENDS IN BRANCH RELAXATION TIMES (τ)

The time constants of each polarization branch are calculated as the product of the branch resistance and capacitance. The physical significance of relaxation times can be interpreted as the time taken for the dipole groups to establish polarization. It can be expressed as a function of temperature as [5]:

$$\tau = \pi \exp \left(\frac{U}{k_B T} \right) / \omega_0 \quad (12)$$

Where, U is the barrier height potential; ω_0 is the angular frequency of particle vibration, T is the absolute temperature and k_B is the Boltzmann Constant. Equation 12 indicates that τ decreases exponentially as temperature increases. Also, with aging, chemical degradation is higher due to depolymerization of cellulose, altering the reaction kinetics and shortening the polarization processes [5]. In Table II, it can be observed that with an increase in temperature and aging degree, τ reduces.

4.5.2 TRENDS IN BRANCH RESISTANCES (R_i)

From the low-frequency dispersion (LFD) theory developed by Jonscher [4], as the temperature decreases, the average kinetic energy of charge carriers contained in the OIP system also declines; rising relaxation times and the LFD frequency descends. Therefore, the resistance decreases with an increase in temperature, which is formulated by Arrhenius Equation [5]:

$$\mu = \mu_0 \exp \left(-E_\mu / k_B T \right) \quad (13)$$

Where, μ is the mobility, E_μ is the activation energy. The reduction in resistance with increasing temperature is due to the mobility of the charge carriers inside the insulation at elevated temperatures. The decreasing trend is prominent in Branch 0, 1, and 2 as observed in Table II and Figure 11. The resistance values provide information about the overall condition of the insulation: higher value indicates better condition of the insulation whereas lower value corresponds to degraded insulation [14].

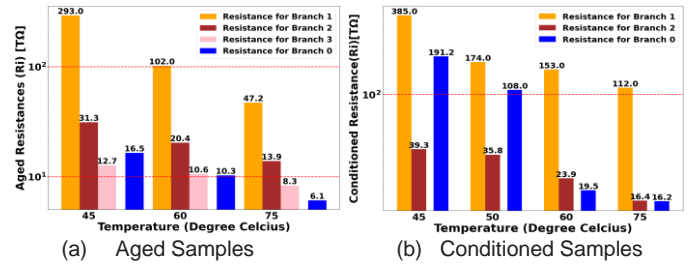


Fig 11. Reduction of branch resistances

4.5.2 TRENDS IN BRANCH CAPACITANCES (C_i)

With the increase in temperature, the capacitance in Branches 1 and 2 increases significantly. This is because the mobility of charge and polar particles, as well as relaxation of dipole groups are retarded, reducing the stored energy in the dipole [5]. This shows a decline in capacitance in the polarization branches. The capacitance in Branches 1 and 2 also increases with the aging degree, which is an indication of a stronger polarization behaviour attributed to the aging possibly by-products like water, organic acids, and furan inside cellulose insulation [12]. For Branch 0 capacitance, the capacitance at 50 Hz is measured and divided by the real part of permittivity and the value is constant as expected. Table 2 and Figure 12 shows this increasing trend of capacitance with temperature for aged samples and a similar trend for conditioned ones but not so strongly.

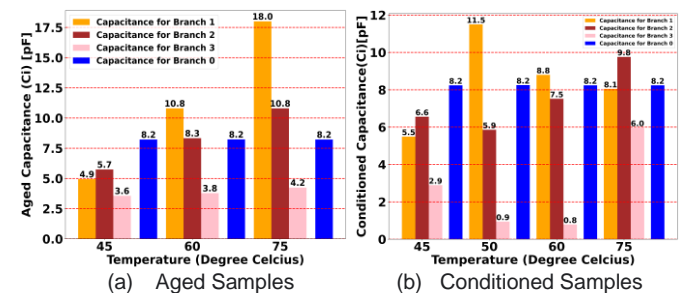


Fig 12. Increase of branch capacitances

According to [5], Feng et. al. has considered 4 branches for modelling their OIP bushing impregnated in the lab using measurements from DIRANA PDC analyzer. The values reveal a very small time constant of 0.46 μ s for Branch 4, which is most likely not possible to measure such polarization times. The first 3 branches provide a time scale in seconds and their obtained values for R and C are in the same magnitude as that obtained in our research. In [9], Xing et. al. performed PDC measurements using the DIRANA testing equipment and validated with 3 branches. The order of magnitude is also similar to the values obtained in our research. In [24], the authors performed PDC measurements and used 3 branches for modelling the OIP which they concluded that it was sufficient to model the possible relaxation processes.

5. PRINCIPLE OF FDS MEASUREMENTS

Figure 13 shows the laboratory implementation of the FDS Measuring System. Three main components of this system are the test cell, IDAX 300 FDS Analyzer, and a PC. The figure shows the dimensions of HV and the measuring electrodes with guard placed inside the temperature oven.

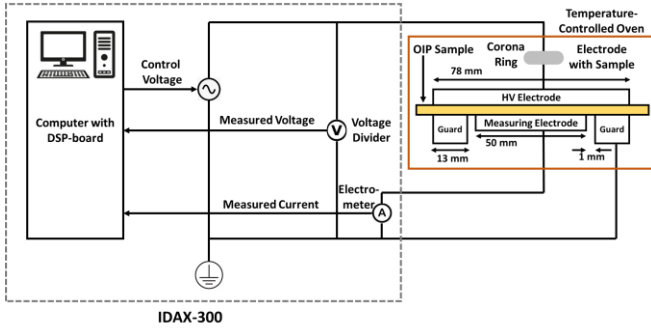


Fig 13. Lab Implementation of FDS measurement system

The IDAX 300 supplies a 200V to the sample which causes a current to flow and the current and voltage signals are measured by the control panel. The test cell comprises the guard electrode as mentioned in Section 4. Different sweeps in frequency were performed and dielectric parameters were obtained for each sweep. So, for a 6-minute sweep, it was observed that an extrapolation model can be constructed predicting values for very low and high frequencies without actual measurements. Thus, it was not required to go to very low frequencies which would result in long measurement times, or to use very high frequencies that would require high charging currents. The model development and the aging parameter have been discussed onwards from Section 5.1.

5.1 FDS MEASURED PARAMETERS

5.1.1 TRENDS IN REAL PERMITTIVITY (ϵ' or K')

The real part of permittivity (ϵ' or K') increases with a decrease in frequency. This phenomenon can be explained by the Debye-Huckel-Falkenhagen theory which states that in disordered systems, the charge transport takes place because of hopping conduction [15,16]. The motion of charge in the system is accompanied by electrical relaxation where ionic or electronic charge is surrounded by negative or positive counter charges. As temperature increases, the degree of polymerization for OIP

Samples reduces and that alters the dielectric characteristics. With the reduction in cellulose polymer chain length in OIP, the real part of permittivity increases [16] as observed in Figure 14.

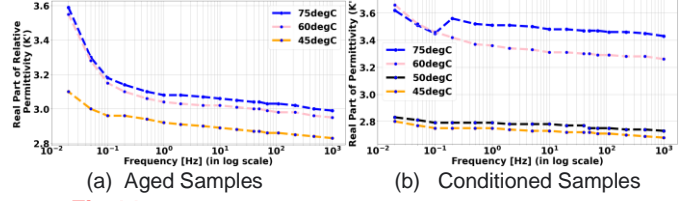


Fig 14. Variation in K' with temperature and aging degree

5.1.2 TRENDS IN IMAGINARY PERMITTIVITY (ϵ'' or K'')

The imaginary part of permittivity (ϵ'' or K'') is observed to first reduce and then increase as frequency increases for both conditioned and aged samples as seen in Figure 15. In the low frequency (0.01-1 Hz) and high frequency (2-10³ Hz), this alternating effect is very prominent. This is because as frequency increases, more polarization processes evolve and the frequency dependence of the conductivity reduces, meaning that dielectric loss is caused by both the conductivity and relaxation process, given by [17]:

$$\tan \delta = \frac{\sigma_0 / \omega \epsilon_0 + \epsilon''}{\epsilon'} \quad (14)$$

Where σ_0 represents the dielectric conductivity and $\tan \delta$ is the loss factor. ϵ'' shows the loss component of the dielectric and as temperature increases, losses also increase shifting the curve upwards. Also, at high frequencies, the electric field changes rapidly and thus the effect of temperature is not visible.

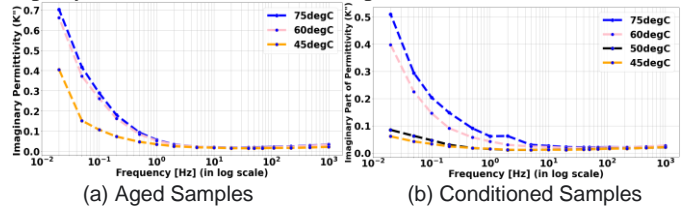


Fig 15. Variation in K'' with temperature and aging degree

5.1.3 TRENDS IN DIELECTRIC LOSSES ($\tan \delta$)

As shown in Equation 13, $\tan \delta$ can be approximated to the ratio of ϵ''/ϵ' . Now from Figures 14 and 15, it is evident that ϵ'' changes more rapidly in the ratio than ϵ' . So, $\tan \delta$ varies according to the trend of ϵ'' . $\tan \delta$ increases with an increase in aging degree possibly as the ionic mobility increases influencing the conductivity of the OIP sample. This increase occurs till 100 Hz, after which there is an increasing trend as seen in Figure 16. This is because at higher frequencies the contribution of the conduction process reduces as observed in Equation 13, where $\omega (=2\pi f)$ increases [16,17].

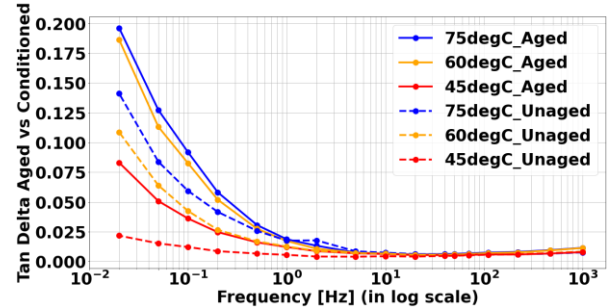


Fig 16. Variation in $\tan \delta$ for aged and conditioned Sample

$\tan\delta_{min}$ is the minimum value at different temperatures showing an increasing trend. This minimum value is reached at low frequencies of 20-40 Hz as shown in Figure 17. This is in good agreement with [25], where $\tan\delta_{min}$ is observed around 30-60 Hz for OIP insulation. Also, at the power frequency of 50 Hz, which is predominantly used in field measurements, aging degree and temperature elevation showed a higher $\tan\delta$ over conditioned ones as in Figure 18.

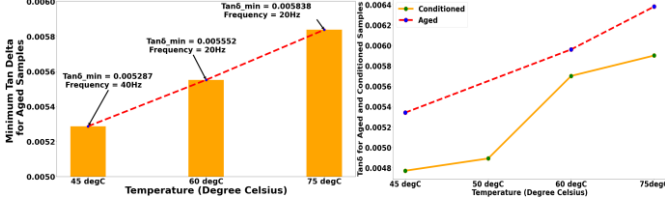


Fig 17, 18. Variation in $\tan\delta_{min}$; Variation in $\tan\delta$ at 50 Hz

5.1.4 RELATIONSHIP BETWEEN IMAGINARY PERMITTIVITY AND POLARIZATION

For very low frequencies (<0.1 Hz for this case), both the parts of the permittivity increase strongly with decreasing frequencies up to significantly high values, clearly indicating electrode polarization. This will mask the dielectric response of the sample and give rise to an unwanted parasitic effect during dielectric measurements. This polarization may be due to conductivity, ambient temperature, or frequencies but they cannot be explained by molecular relaxation processes [16]. At slightly higher frequencies of 0.1-1 Hz, ϵ' remains almost constant whereas ϵ'' reduces with frequency increment, which means dielectric loss is mainly due to conductivity contribution. When $\log(\epsilon'')$ vs $\log(f)$ is plotted as seen in Figure 19, it is observed that they have a linear relationship whose slope is affected by the Maxwell-Wagner process [16]. Beyond 1 Hz, ϵ'' is observed to increase whereas ϵ' reduces with an increase in frequency. This is the relaxation process generated by the polarization of dipoles and separation of charges at oil-paper interfaces. Thus, the whole frequency domain dielectric permittivity at constant temperature can be divided into the 3 mentioned parts as seen in Figure 20. With temperature change, it is expected that the polarization process and conductivity would be affected; thereby the Cole-Cole Model would help in identifying aging characteristics in OIP samples [26].

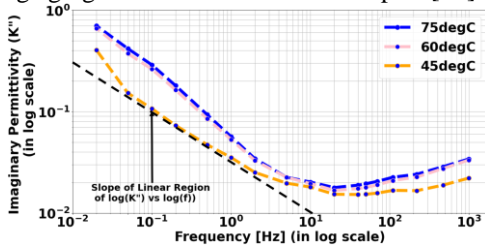


Fig 19. Slope in low frequency of $\log(\epsilon'')$ vs $\log(f)$

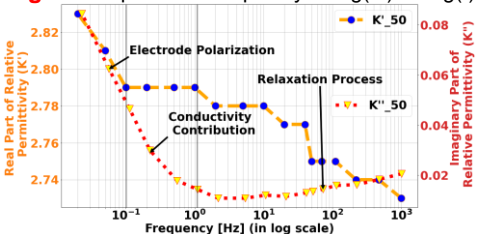


Fig 20. Variation of K' vs K'' for conditioned sample at 45°C

5.2 DERIVING THE COLE-COLE MODEL

Consider the impedance of insulation ($Y(s)$) in the s-domain, as seen in Equation (14), where C_{∞} and C_s are the capacitance at very high and low frequencies respectively. Then the Cole-Cole Model equivalent electrical circuit [26] by Equations (16, 17) can be represented as shown in Figure 21. The geometric interpretation of the model from Figure 21 enables us to derive the linear fit between $\ln |v/u|$ vs $\ln(f)$.

$$Y(s) = sC_{\infty} + \frac{(C_s - C_{\infty})s}{1 + (s\tau)^{1-\alpha}} = sC_{\infty} + \frac{1}{Z_1(s)} \quad (15)$$

$$Z_1(s) = \frac{(s\tau)^{\alpha} + s\tau}{(C_s + C_{\infty})(s\tau)^{\alpha}} = \frac{1}{(C_s - C_{\infty})s} + Z_a(s) \quad (16)$$

$$Z_a(s) = \frac{\tau}{(C_s + C_{\infty})(s\tau)^{\alpha}} \quad (17)$$

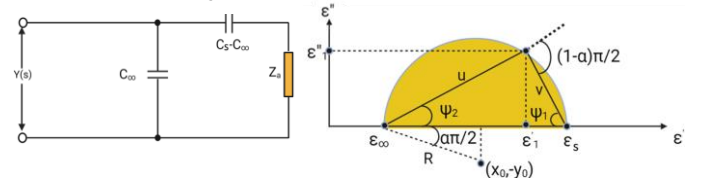


Fig 21. Cole-Cole model circuit, Geometric representation of OIP based Cole-Cole model

From geometric model, value of triangle sides v and u [27]:

$$u = \sqrt{(\epsilon'_1 - \epsilon_{\infty})^2 + \epsilon_1'^2}; v = \sqrt{(\epsilon_s - \epsilon'_1)^2 + \epsilon_1'^2} \quad (18)$$

$$\left|\frac{u}{v}\right| = (\omega\tau)^{1-\alpha}; \text{Arg}(v) - \text{Arg}(u) = (1-\alpha)\frac{\pi}{2} \quad (19)$$

Calculating the α coefficient and then evaluating τ [26]:

$$\alpha = 1 - \frac{2}{\pi}(\psi_1 + \psi_2) = 1 - \frac{2}{\pi}\left(\tan^{-1} \frac{\epsilon_1''}{\epsilon_s - \epsilon'_1} + \tan^{-1} \frac{\epsilon_1''}{\epsilon'_1 - \epsilon_{\infty}}\right) \quad (20)$$

$$\tau = \frac{1}{\omega} \left[\frac{(\epsilon_s - \epsilon'_1)^2 + \epsilon_1'^2}{(\epsilon'_1 - \epsilon_{\infty})^2 + \epsilon_1'^2} \right] \quad (21)$$

Rewriting Equation 20 to 21 and taking logarithm, we obtain:

$$\tau\omega^{(1-\alpha)} = \left[\frac{(\epsilon_s - \epsilon'_1)^2 + \epsilon_1'^2}{(\epsilon'_1 - \epsilon_{\infty})^2 + \epsilon_1'^2} \right]^{0.5} \quad (22)$$

$$\Rightarrow (1-\alpha)\log_e \tau + (1-\alpha)\log_e \omega = 0.5\log_e \frac{|v|}{|u|} \quad (23)$$

5.3 COLE-COLE MODEL FITTING ALGORITHM

Step 1: Acquiring the Real Part of Permittivity

For all the temperatures and aging degrees, the real part of permittivity(ϵ') is extracted from a short sweep of frequency from 0.01-10³ Hz equaling a time of 6 minutes.

Step 2: Mathematical Model to find ϵ_{∞} and ϵ_s

From literature [28], a power model best fits the data with minimum Residual Error and best R^2 scores. For all the conditions, the function was obtained of the form $\epsilon' = A\omega^{f-B}$, and using this the value at $f = 1\mu\text{Hz}$ and 1 kHz is predicted. Higher frequencies are not chosen since the curve almost reaches constant at higher frequencies and thus, there are not a lot of deviations in the model predicted values.

Step 3: Fitting the Cole-Cole Model to Extract Parameters

Equation (23) is applied to the obtained data from Step 2 to obtain the values of α and τ . The goodness of fit for Steps 2 and 3 shows a very high value indicating how well the model fits on data as shown in Table III.

TABLE III
PARAMETER ESTIMATION FOR POWER AND LINEAR FITS

Temperature	Power Curve Fit for ϵ'	Linear Fit for Cole-Cole Model
45°C	$R^2 = 0.9526$ $SSE = 0.000663$ $\epsilon'_d = 2.87$ $\epsilon'_{\infty} = 2.68$	$R^2 = 0.97$ $SSE = 0.1955$ $Slope = 0.1659$ $Intercept = 1.232$
50°C	$R^2 = 0.9317$ $SSE = 0.0008183$ $\epsilon'_d = 2.96$ $\epsilon'_{\infty} = 2.73$	$R^2 = 0.9222$ $SSE = 0.6432$ $Slope = 0.1752$ $Intercept = 1.197$
60°C	$R^2 = 0.91$ $SSE = 0.01232$ $\epsilon'_d = 3.96$ $\epsilon'_{\infty} = 3.26$	$R^2 = 0.9532$ $SSE = 0.8012$ $Slope = 0.26$ $Intercept = 1.705$
75°C	$R^2 = 0.40$ $SSE = 0.014$ $\epsilon'_d = 3.85$ $\epsilon'_{\infty} = 3.43$	$R^2 = 0.971$ $SSE = 0.3198$ $Slope = 0.278$ $Intercept = 1.68$

5.4 TRENDS IN MODEL DERIVED PARAMETERS AND RESULTS

5.4.1 TRENDS IN TIME CONSTANT (τ)

As observed in PDC Measurements, the time constants reduce similar to PDC with temperature and aging degree as seen in Figure 22(a), because increasing temperature interferes with the ordering of the dipole, reducing the value of τ [26]. The values are much reduced in this case since this is a 6-minute analysis over the 3 hours PDC, which allowed the slow polarization processes to complete and reflect on the output current.

5.4.2 TRENDS IN ALPHA (α)

α depends on the structure of the dipole particles participating in polarization [26]. With temperature variation, orientation polarization takes place altering the chemical structure. With the increase in temperature and aging degree, the coefficient also decreases but this change is not very significantly observable (Figure 22(b)).

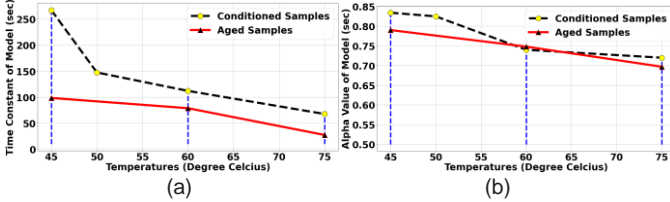


Fig 22. Variation of (a) Time constant, (b) Alpha parameter

6 CONCLUSIONS

The paper discusses the sudden temperature rise trends in the field-installed HPGC cables, raising the operating temperature from 30 to 42°C. This motivates our study to understand the effect of this change on insulation parameters on samples obtained from field-aged cables. This implies that the samples have already undergone degradation from field use and the effect of temperature rise (Figure 1) needs to be understood well. The novel electronics circuit developed at TU Delft provides a very low-cost alternative to commercial systems which has been validated with known samples beforehand. Also, the PDC model parameters obtained from this research hold a good agreement with state-of-art literature which mostly uses samples made in lab. Using the error function approach, the model complexity is reduced yet critical information is not lost for modeling. The optimal branches for used OIP samples were evaluated to be 3 along with the geometric branch. On the already-aged samples, an increase in temperature and degree of aging shows an increase in DC conductivity, and polarization currents and reduces the decay rates of depolarization currents. The results reveal even after decades of field operation, it is still possible to detect significant changes in the model parameters varying with temperature, where the

model branch resistances and time constants are observed to reduce whereas the capacitance increases. Branch resistances for aged samples show a high 65% reduction from 45°C to 60°C and 54% from 60°C to 75°C for the main Branch 1. Conditioned samples showed 60% from 45°C to 60°C and 27% at 60°C to 75°C. For branch capacitances, aged samples showed 55% from 45°C to 60°C whereas 40% at 60°C to 75°C. For conditioned samples, from 45°C to 60°C the increase is 38%, and it is -8% from 60°C to 75°C. Therefore, the capacitance change is more prominent in aged samples due to more aging time than in conditioned ones. Also, the resistance variation seems to be more prominent than the capacitance change.

From the FDS measurements, an increment in temperature reflects an increase in $\tan\delta$ by 10% and 6.7% from 45°C to 60°C and from 60°C to 75°C respectively in aged samples. In conditioned samples, increase is by 14% and 4% from 45°C to 60°C and from 60°C to 75°C respectively. The parameters from PDC and FDS measurements with temperature is also reflected in the breakdown voltages for different temperatures. Long-term stress tests were performed on the aged samples which produced reliable breakdown statistics and the Maximum Likelihood Estimation of Inverse Power Law was fitted on 2-parameter Weibull distributed breakdown data. The modeling of the final log-likelihood function with complete and right censored data was computed to be as in Equation (24) which is used to solve for model variables [29].

$$\Lambda = \sum_{i=1}^{N_c} n_i \ln \left[\beta K S_i^n (K S_i^n t_i)^{\beta-1} e^{-(K S_i^n t_i)^{\beta}} \right] - \sum_{j=1}^{N_r} n_j (K S_j^n t_j)^{\beta} \quad (24)$$

Where, N_c is the number of samples constituting complete failure data set and N_r represents the right censored data, β is the shape parameter from Weibull Distribution, K is the constant of proportion in power law, S is the voltage stress and n is the power in power law and t represents the time to failure. Among the variables, the exponent of power law showed a monotonic reduction with increase in temperature, indicating a significant non-linear decrease in the electrical life of the insulation with increase in temperature.

TABLE III

LIFE MODEL EXPONENT VARIATION WITH TEMPERATURE

Temperature	45 °C	60 °C	75 °C
n -parameter	13.61	10.81	7.38

The FDS model has been based on short time permittivity extrapolation method which greatly reduces the measurement times showing relaxation times and alpha parameter decreasing with an increase in aging degree and temperature. All the discussed parameters show a very strong correlation, either positive or negative, indicating an increasing or decreasing trend respectively, with temperature and aging as shown in Figure 23 (only conditioned samples) as a heatmap by analyzing the Pearson's Correlation Coefficient (r).

For aged samples, the correlation values tend to be more extreme, indicating a stronger effect of parameter variation with the aging degree. Thus, for the OIP Cables, the values can be monitored over time to indicate the degradation of cable insulation based on the parameter trends. For the replacement strategy, these non-destructive methods are to be implemented, and then a relative comparison of the highly correlated parameters would enable to differentiate their conditions.

IEEE TRANSACTIONS ON DIELECTRICS AND ELECTRICAL INSULATION

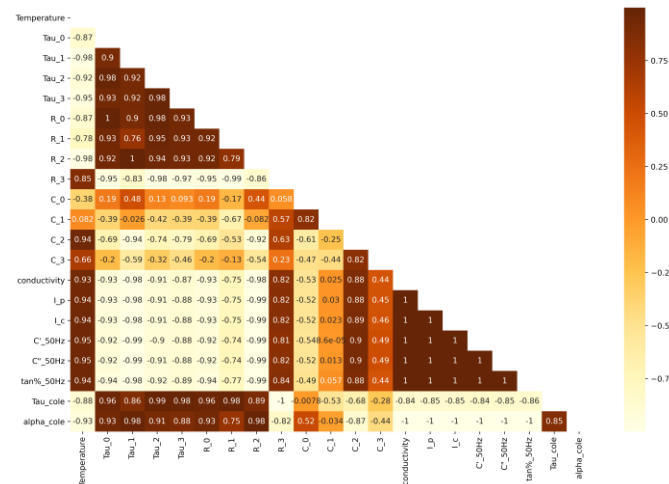


Fig 23. Heat map correlation for conditioned samples

REFERENCES

- [1] Wang, Y., Zhao, A., Zhang, X., Shen, Y., Yang, F., Deng, J., & Zhang, G. (2016, September). Study of dielectric response characteristics for thermal aging of XLPE cable insulation. In *2016 International Conference on Condition Monitoring and Diagnosis (CMD)* (pp. 602-605). IEEE.
- [2] T. K. Saha, P. Purkait and F. Muller, "Deriving an equivalent circuit of transformers insulation for understanding the dielectric response measurements," in *IEEE Transactions on Power Delivery*, vol. 20, no. 1, pp. 149-157, Jan. 2005, doi: 10.1109/TPWRD.2004.835436.
- [3] G. Frimpong, U. Gafvert and J. Fuhr, "Measurement and modeling of dielectric response of composite oil/paper insulation," *Proceedings of 5th International Conference on Properties and Applications of Dielectric Materials*, 1997, pp. 86-89 vol.1, doi: 10.1109/ICPADM.1997.617534.
- [4] Andrew K Jonscher. Dielectric relaxation in solids. *Journal of Physics D: Applied Physics*, 32(14): R57, 1999.
- [5] Yang, Feng, Lin Du, Lijun Yang, Chao Wei, Youyuan Wang, Liman Ran, and Peng He. 2018. "A Parameterization Approach for the Dielectric Response Model of Oil Paper Insulation Using FDS Measurements" *Energies* 11, no. 3: 622. <https://doi.org/10.3390/en11030622>
- [6] C. Stancu, P. V. Notinger and L. V. Badicu, "Dielectric response function for nonhomogeneous insulations," *2011 Annual Report Conference on Electrical Insulation and Dielectric Phenomena*, 2011, pp. 97-100, doi: 10.1109/CEIDP.2011.6232605.
- [7] X. Ji Quan, Y. Lijun, L. Bin, L. Ruijin, H. Yunhua and G. Pei, "Study on assessing the ageing condition of oil paper insulation by Polarization/Depolarization current," *2013 Annual Report Conference on Electrical Insulation and Dielectric Phenomena*, 2013, pp. 617-621, doi: 10.1109/CEIDP.2013.6747068.
- [8] Aging Model and Parameter Determination for High Pressure Gas Cables at Elevated Electro-Thermal Stress, Devayan Basu, <http://resolver.tudelft.nl/uuid:d6acf721-58ee-4dd6-b92a-4c28c9168be2>
- [9] Xing Zhang, Long Xu, Aixuan Zhao, Yanbo Wang, XueFeng Zhao, Lu Pu, Junbo Deng, and Guanjun Zhang. "Research on conversion of polarization/depolarization current and frequency domain spectroscopy for XLPE cable," *2017 1st International Conference on Electrical Materials and Power Equipment (ICEMPE)*, 2017, pp. 452-456, doi: 10.1109/ICEMPE.2017.7982126.
- [10] Morsalin, Sayidul & Sahoo, Animesh & Phung, Toan. (2019). "Recovery Voltage Response of XLPE Cables Based on Polarisation and Depolarisation Current Measurements", *IET Generation, Transmission & Distribution*. 13. 10.1049/iet-gtd.2019.1004.
- [11] Vahidi, F., Tenbohlen, S., Rösner, M., Perrier, C., & Fink, H. (2013, November). The investigation of the temperature and electric field dependency of mineral oil electrical conductivity. In *Proceedings of the ETG Power Engineering Society Symposium, Dresden, Germany* (Vol. 12).
- [12] Thomas A Prevost. "Thermally upgraded insulation in transformers", In *Proceedings Electrical Insulation Conference and Electrical Manufacturing Expo*, 2005., pages 120–125. IEEE, 2005.

- [13] X. Zhongnan. Study on simulation and experiment of polarization and depolarization current for Oil paper insulation ageing. Master's Thesis, 2011.
- [14] Fofana, I., Hemmatjou, H., Meghnefi, F., Farzaneh, M., Setayeshmeh, A., Borsi, H., & Gockenbach, E. (2009, May). Low temperature and moisture effects on oil-paper insulation dielectric response in frequency domain. In *2009 IEEE Electrical Insulation Conference* (pp. 368-372). IEEE.
- [15] Jeppe C Dyre. The random free energy barrier model for ac conduction in disordered solids. *Journal of Applied Physics*, 64(5):2456–2468, 1988
- [16] Ming Dong, Ming Ren, Fuxin Wen, Chongxing Zhang, Jialin Liu, Christof Sumereder, and Michael Muhr. "Explanation and analysis of oil paper insulation based on frequency domain dielectric spectroscopy." *IEEE Transactions on Dielectrics and Electrical Insulation*, 22(5):2684–2693, 2015.
- [17] Chunshu Xu, Shi Qiang Wang, Hao Xu, and Guan Jun Zhang. "Temperature effect on frequency domain spectroscopy characteristics of oil impregnated pressboard", *Proceedings of 2011 International Symposium on Electrical Insulating Materials*, pages 197–200. IEEE, 2011.
- [18] Chuanhui Cheng, Kai Wu, Mingli Fu, YanPeng Hao, Shuangzan Ren, Jingfeng Wu, and Hao Wu. "Interface charge barrier between oil and oil immersed paper." *IEEE Transactions on Dielectrics and Electrical Insulation*
- [19] Żukowski, P., Kołtunowicz, T.N., Kierczyński, K. *et al.* "Permittivity of a composite of cellulose, mineral oil, and water nanoparticles: theoretical assumptions." *Cellulose* 23, 175–183 (2016).
- [20] Zhiguo Ding and Minrui Fei. "An anomaly detection approach based on isolation forest algorithm for streaming data using sliding window." *IFAC Proceedings Volumes*, 46(20):12–17, 2013. 3rd IFAC Conference on Intelligent Control and Automation Science ICONS 2013.
- [21] Electric cables calculation of the current rating part 11: Current rating equations (100 % load factor) and calculation of losses general. IEC 6028711: 2006, 41(3):65, 20061213.
- [22] Electric cables calculation of the current rating part 21: Thermal resistance calculation of the thermal resistance. IEC 6028721: 2015, 3(3):84, 20150409.
- [23] Bozdogan, H. "Model selection and Akaike's Information Criterion (AIC): The general theory and its analytical extensions". *Psychometrika* 52, (1987)
- [24] Shayegani, A. A., Omar Hassan, H. Borsi, E. Gockenbach, and H. Mohseni. "PDC measurement evaluation on oil-pressboard samples." In *Proceedings of the 2004 IEEE International Conference on Solid Dielectrics*, 2004. ICSD 2004., vol. 1, pp. 51-54. IEEE, 2004.
- [25] Dutta, S., Mukherjee, M., Pradhan, A. K., Baral, A., & Chakravorti, S. (2016, December). Effect of temperature on condition assessment of oil-paper insulation using polarization-depolarization current. *2016 National Power Systems Conference (NPSC)* (pp. 1-5). IEEE.
- [26] Stefan Wolny, Artur Adamowicz, and Marek Lepich. "Influence of temperature and moisture level in paper oil insulation on the parameters of the cole-cole model." *IEEE Transactions on Power delivery*, 29(1):246–250, 2013.
- [27] Bishay, Samiha T. "Numerical methods for the calculation of the Cole-Cole parameters." *Physics department, AimShams University, Cairo, Egypt* (2000).
- [28] Dai, Quanmin, Yanxia Liu, and Guang Cheng. "The mathematical model of dissipation factor with temperature–frequency effect for oil-impregnated paper bushings." *AIP Advances* 10.11 (2020): 115112.
- [29] Devayan Basu, Babak Gholizad, Robert Ross, Shima Mousavi Gargari, "Temperature Effect on Electrical Aging Model for Field-Aged Oil Impregnated Paper Insulation", *IEEE Conference on Electrical Insulation and Dielectric Phenomena (CEIDP)*, 2022. (Accepted yet to be published)